A DIMENSIONAL SPLITTING METHOD FOR NONLINEAR EQUATIONS WITH VARIABLE COEFFICIENTS

KNUT–ANDREAS LIE

ABSTRACT. A numerical method is presented for the variable coefficient, nonlinear advection equation $u_t + \sum_{i=1}^{d} V_i(x,t) f_i(u)_{x_i} = 0$ in arbitrary space dimension for bounded velocities that are Lipschitz continuous in the x variable. The method is based on dimensional splitting and uses a recent front tracking method to solve the resulting one-dimensional non-conservative equations. The method is unconditionally stable, and it produces a subsequence that converges to the entropy solution as the discretization of time and space tends to zero. Three numerical examples are presented.

1. INTRODUCTION

We consider variable coefficient, hyperbolic equations of the form

$$u_t + \sum_{i=1}^{d} V_i(x,t) f_i(u)_{x_i} = 0, \qquad u(x,0) = u_0(x). \tag{1}$$

An important example is nonlinear advection of a scalar quantity u in a specified velocity field $V(x,t)$ in arbitrary space dimension. If the flow is incompressible, the conservation law governing the process can be written in the non-conservative form (1). This type of equation is frequently occurring in simulation of flow phenomena. An important application—which was the initial motivation for this study—is the modelling of displacement of oil by water in petroleum reservoirs. In this case the flux function has a typical s-shape and the initial value problem is sometimes called a Buckley–Leverett problem. Other applications are containment transport in saturated groundwater flow, atmospheric models of trace gases, and models for chemical reactors. The equation also occurs when simulation advection processes on curvilinear grids.

In the following we will develop a numerical method for (1). The development is strongly inspired by a dimensional splitting method proposed by Holden and Risebro [5] for the constant coefficient equation $u_t + \sum_{i=1}^{d} f_i(u)_{x_i} = 0$. Dimensional splitting decomposes the problem into a series of one-dimensional problems, one in each direction, and is a widely used technique to extend one-dimensional numerical methods to multi-dimensional problems. Holden and Risebro used a very efficient front tracking method [4] to solve the one-dimensional equations, and thus obtained a numerical method that is unconditionally

Date: October 13, 1997.

Key words and phrases. multi-dimensional advection, variable coefficients, dimensional splitting, front tracking, scalar conservation laws.

My research has been supported by the Research Council of Norway under grant 100555/410.

stable and very efficient [10]. The front tracking method has recently [9] been extended to the variable coefficient equation

$$u_t + V(x,t)f(u)_x = 0, \qquad u(x,0) = u_0(x). \tag{2}$$

We use this new method as a building block for generalizing Holden and Risebro's method to the variable coefficient equation (1). See Ref. [8] and the references therein for other approaches, mainly for linear flux functions, for which our method coincides with the method of characteristics.

The outline of the paper is as follows. §2 describes the construction of approximate solutions, and thereby introduces the numerical method implicitly. In §3 we verify that the approximate solutions converge to the entropy weak solution. Finally, three numerical experiments are presented in §4: two simple linear advection problems and a model problem from two–phase reservoir flow.

2. Construction of Approximate Solutions

For simplicity, the dimensional splitting method will be presented for an equation in two spatial dimensions with time independent velocity field. That is, we consider the equation

$$u_t + U(x,y)f(u)_x + V(x,y)g(u)_y = 0, \qquad u(x,y,0) = u_0(x,y). \tag{3}$$

It is straightforward to generalize the method to higher dimensions and time dependent velocities.

Our interest is with solutions that may contain discontinuities. Existence and uniqueness of discontinuous solutions were proved by Kružkov [7], who also proposed an *entropy condition* to identify the unique physical solution, see §3. Let $u(t) = \mathcal{S}(t)u_0$ denote the entropy solution of (3). Then dimensional splitting approximations can be defined as

$$\mathcal{S}(n\Delta t)u_0(x,y) \cong \left[\mathcal{S}^{g,V}(\Delta t)\mathcal{S}^{f,U}(\Delta t)\right]^n u_0(x,y), \qquad \text{(Godunov)}$$

$$\mathcal{S}(n\Delta t)u_0(x,y) \cong \left[\mathcal{S}^{f,U}(\Delta t/2)\mathcal{S}^{g,V}(\Delta t)\mathcal{S}^{f,U}(\Delta t/2)\right]^n u_0(x,y), \qquad \text{(Strang)}$$

where $\mathcal{S}^{f,U}(t)u_0$ and $\mathcal{S}^{g,V}(t)u_0$ are the exact solutions of (2) with flux functions f and g and velocities U and V, respectively.

Here we consider numerical approximations defined on a uniform Cartesian grid with nodes $\{(i\Delta x, j\Delta y)\}$, where $\Delta x, \Delta y$ are given positive numbers and $i,j \in \mathbf{Z}$. The one-dimensional solution operators will be approximated using front tracking for equation (2).

One-Dimensional Front Tracking. In the front tracking method for (2) we seek to construct an approximation within the class of piecewise constant functions (step functions). First the initial data u_0 are approximated by a step function. This defines a sequence of local Riemann problems. If the flux function f is approximated by a piecewise linear function, the similarity solution of each Riemann problem is again a step function. Each discontinuity (or front) in the Riemann solution propagates along a path $x(t)$ described by an ordinary differential equation $\dot{x} = V(x)s$, where s is the Rankine–Hugoniot velocity $s = (f(u^+) - f(u^-))/(u^+ - u^-)$. If we approximate the velocity by a piecewise linear function, each differential equation can be solved explicitly. The local Riemann problems are then connected, and we track the outgoing fronts up to the time of the first wave interaction. This interaction is a new Riemann problem which is solved by a step function, and so on. The front tracking algorithm thus consists of solving Riemann problems and tracking fronts until they collide. The method is first order and has no associated time step [9]. If the velocity is time dependent, the algorithm is essentially the same, except that special care should be taken when the velocity changes sign in time, see Lie [9]. (The velocity approximation is now, for instance, piecewise constant in time).

Dimensional Splitting. Let π be the usual grid block averaging operator defined on the uniform grid $\{(i\Delta x, j\Delta y)\}$; that is,

$$\pi u(x,y) = \frac{1}{\Delta x \Delta y} \iint\limits_{z_{i,j}} u(\xi,\eta)\, d\xi d\eta, \qquad \forall (x,y) \in z_{i,j}, \tag{4}$$

where $z_{i,j}$ is grid block number (i,j) with lower left-hand corner in $(i\Delta x, j\Delta y)$. This projection has the property that $\iint |\pi u - u| = \mathcal{O}(\max(\Delta x, \Delta y))$. For the velocity approximations U^δ, V^δ we assume that U^δ (V^δ) is piecewise linear in the x-direction (y-direction) and piecewise constant in the y-direction (x-direction). Furthermore, assume that $\|U^\delta_{j+1} - U^\delta_j\|_\infty \le C_U \Delta y$ and $\|V^\delta_{i+1} - V^\delta_i\|_\infty \le C_V \Delta x$ for positive constants C_U, C_V.

Now, let $\mathcal{S}^{f,U}_\delta(t)$ and $\mathcal{S}^{g,V}_\delta(t)$ denote the front tracking solution operators. Using Godunov splitting, the dimensional splitting solution $\{u^n_{ij}\}_{n=1}^N$ is then defined as

$$u^n_{ij}(x,y) = \left[\pi \mathcal{S}^{g,V}_\delta(\Delta t) \pi \mathcal{S}^{f,U}_\delta(\Delta t)\right]^n \pi u_0(x,y). \tag{5}$$

The approximate solution is defined analogously for the Strang splitting, and the extension to arbitrary space dimension is obvious.

3. Convergence to the Entropy Solution

The one-dimensional solutions constructed by front tracking have the three following important properties [9, Lemma 2.3]: Suppose that f is continuous and piecewise linear, V is bounded, and u_0 is a bounded step function with finite total variation. Moreover, assume that for each finite $T > 0$ there are a finite number of τ's less than T such that $\operatorname{sgn} V(x,\tau^-) \ne \operatorname{sgn} V(x,\tau^+)$, and assume that $\operatorname{sgn} V(a^+,t) = \operatorname{sgn} V(a^-,t)$ at every point of discontinuity (a,t). Then the solution of $u_t + V(x,t) f(u)_x = 0$ satisfies

(1) a maximum principle, $\|u\|_\infty \le \|u_0\|_\infty$,
(2) Lipschitz continuity of the L^1-norm, $\|u(t_2) - u(t_1)\|_1 \le C|t_2 - t_1|$,
(3) TVD-property, $\mathrm{TV}(u) \le \mathrm{TV}(u_0)$.

We will now prove that the dimensional splitting solution has the same three properties. This will in turn ensure the existence of a convergent subsequence. For convenience we assume that $\Delta x = C_1 \Delta y = C_2 \Delta t$, for nonzero constants C_1, C_2.

Lemma 3.1. *The solution $u^n(x,y)$ remains bounded in time, $\|u^n(x,y)\|_\infty \le \|u_0(x,y)\|_\infty$.*

Proof. The one-dimensional solution operators $\mathcal{S}^{f,U}_\delta$ and $\mathcal{S}^{g,V}_\delta$ do not introduce new maxima or minima into the solution, and neither does the projection operator π. □

Lemma 3.2. *If u_0 has compact support, then there is a positive constant C such that*

$$\sum_{ij} |u_{ij}^m - u_{ij}^n| \Delta x \Delta y \leq \big[C\Delta t + \mathcal{O}\big(\max(\Delta x, \Delta y)\big)\big] \, |m-n|.$$

Proof. The lemma follows by induction if we can prove that

$$\sum_{ij} |u_{ij}^{n+1} - u_{ij}^n| \Delta x \Delta y \leq C\Delta t + \mathcal{O}\big(\max(\Delta x, \Delta y)\big).$$

One time step in our algorithm can be described as

$$u_{ij}^n = u_j^n(0) \xrightarrow{\mathcal{S}_\delta^{f,U}} u_j^n(\Delta t) \xrightarrow{\pi} u_{ij}^{n+\frac{1}{2}} = u_i^{n+\frac{1}{2}}(0) \xrightarrow{\mathcal{S}_\delta^{g,V}} u_i^{n+\frac{1}{2}}(\Delta t) \xrightarrow{\pi} u_{ij}^{n+1}.$$

The L^1-norm of the one-dimensional front tracking solution is Lipschitz continuous in time, and hence we see that

$$\sum_k |u_j^n(\xi_k, \Delta t) - u_j^n(\xi_k, 0)|(x_{k+1} - x_k) \leq D\Delta t,$$

where $\xi_k \in [x_k, x_{k+1}]$ and the intervals $\{[x_k, x_{k+1}]\}$ are given such that *both* $u_j^n(x, \Delta t)$ and $u_j^n(x, 0)$ are constant on each interval. A similar inequality is valid for the y-sweep from $u_i^{n+1/2}(0)$ to $u_i^{n+1/2}(\Delta t)$. For convenience we assume that the compact support of u^n for all finite n is embedded in the rectangle with corners $x = \pm N\Delta x$ and $y = \pm M\Delta y$. This is a reasonable assumption, as u^0 has finite support and all waves propagate with finite speed. Using the above inequality and the properties of the projection operator now gives

$$\begin{aligned}
\sum_{ij} |u_{ij}^{n+1} - u_{ij}^n| \Delta x \Delta y \leq & \iint_{\mathbf{R}^2} |u_{ij}^{n+1} - u_i^{n+\frac{1}{2}}(\Delta t)| \, dxdy + \iint_{\mathbf{R}^2} |u_{ij}^{n+\frac{1}{2}} - u_j^n(\Delta t)| \, dxdy \\
& + \sum_{i=-N}^{N} \Delta x \sum_k |u_i^{n+\frac{1}{2}}(\eta_k, \Delta t) - u_i^{n+\frac{1}{2}}(\eta_k, 0)|(y_{k+1} - y_k) \\
& + \sum_{j=-N}^{N} \Delta y \sum_k |u_j^n(\xi_k, \Delta t) - u_j^n(\xi_k, 0)|(x_{k+1} - x_k) \\
\leq & C\Delta t + \mathcal{O}\big(\max(\Delta x, \Delta y)\big).
\end{aligned}$$

□

Lemma 3.3. *There is a constant C such that* $\mathrm{TV}(u^n) \leq e^{Cn\Delta t}\,\mathrm{TV}(u_0)$*; that is, the total variation of the solution $u^n(x, y)$ is finite in finite time.*

Proof. Using induction, it is sufficient to prove that $\mathrm{TV}(u^{n+1}) \leq e^{C\Delta t}\,\mathrm{TV}(u^n)$. The total variation for a two-dimensional function $v(x, y)$ can be written

$$\mathrm{TV}(v(\cdot,\cdot)) = \int_{\mathbf{R}} \mathrm{TV}_x(v(\cdot, y)) \, dy + \int_{\mathbf{R}} \mathrm{TV}_y(v(x, \cdot)) \, dx.$$

Let us first consider the x-sweep of the algorithm. The front tracking solution is total variation diminishing by construction. If v is a step function, then $\mathrm{TV}_x(\pi v) \le \mathrm{TV}_x(v)$, and we get that

$$\sum_i |u_{i+1,j}^{n+\frac12} - u_{ij}^{n+\frac12}| \le \sum_i |u_{i+1,j}^n - u_{ij}^n|. \tag{6}$$

Let v denote the solution of $v_t + U(x)f(u)_x = 0$ with initial data v_0 and w the solution of $w_t + V(x)f(u)_x = 0$ with initial data w_0. Then we have that [9, Lemma 3.2]

$$\|v(\cdot,t) - w(\cdot,t)\|_{L^1(\mathbf{R})} \le e^{\gamma t}\|v_0 - w_0\|_{L^1(\mathbf{R})} + te^{\gamma t}\|f\|_{\mathrm{Lip}}\|U - V\|_\infty \mathrm{TV}(v_0),$$

for some constant γ. Now let $v = u_j^n(x,\Delta t)$ and $w = u_{j+1}^n(x,\Delta t)$ be two step functions obtained by front tracking in tube j and $j+1$, respectively. The corresponding velocities are $U_j(x)$ and $U_{j+1}(x)$. Assume that u and v are constant on the intervals $\{[x_k, x_{k+1}]\}$. If $\xi_k \in [x_k, x_{k+1}]$, then

$$\begin{aligned}\int_{\mathbf{R}} |u_{j+1}^n(x,\Delta t) - u_j^n(x,\Delta t)|\,dx &\equiv \sum_k |u_{j+1}^n(\xi_k,\Delta t) - u_j^n(\xi_k,\Delta t)|(x_{k+1} - x_k)\\ &\le e^{\gamma\Delta t}\sum_i |u_{i,j+1}^n - u_{ij}^n|\Delta x + \Delta t e^{\gamma\Delta t}\|f\|_{\mathrm{Lip}} C_U \Delta y\,\mathrm{TV}_x(u_{\cdot,j}^n).\end{aligned}$$

After applying the projection operator we have that

$$\sum_i |u_{j+1}^{n+\frac12} - u_j^{n+\frac12}|\Delta x = \sum_k |u_{j+1}^n(\xi_k,\Delta t) - u_j^n(\xi_k,\Delta t)|(x_{k+1} - x_k),$$

and hence

$$\begin{aligned}\sum_i |u_{j+1}^{n+\frac12} - u_j^{n+\frac12}|\Delta x \le{}& e^{\gamma\Delta t}\sum_i |u_{i,j+1}^n - u_{ij}^n|\Delta x\\ &+ \Delta t e^{\gamma\Delta t}\|f\|_{\mathrm{Lip}} C_U \Delta y\,\mathrm{TV}_x(u_{\cdot,j}^n).\end{aligned} \tag{7}$$

Summing (7) and (6) times Δy over j and adding the result gives

$$\begin{aligned}\mathrm{TV}(u^{n+\frac12}) &\le \int_{\mathbf{R}} \mathrm{TV}_x(u^n)\,dy + e^{\gamma\Delta t}\int_{\mathbf{R}} \mathrm{TV}_y(u^n)\,dx + \Delta t\|f\|_{\mathrm{Lip}}\|U\|_{\mathrm{Lip}} e^{\gamma\Delta t}\int_{\mathbf{R}} \mathrm{TV}_x(u^n)\,dy\\ &\le (1 + \lambda\Delta t)e^{\gamma\Delta t}\,\mathrm{TV}(u^n).\end{aligned}$$

A similar results holds for the y-sweep. Using the fact that $(1+a) \le e^a$ for positive a gives that $\mathrm{TV}(u^{n+1}) \le e^{C\Delta t}\,\mathrm{TV}(u^n)$. □

Assume first that u^0 has compact support. Let Δ denote all the discretization parameters, $\Delta = (\Delta x, \Delta y, \delta, \Delta t)$. Then the construction in §2 gives a family $\{u_\Delta(t)\}$ of approximate solutions. We can now show that the sequence $\{u_\Delta(t)\}$ is convergent by using Lemmas 3.1–3.3 and Helly's theorem, see Crandall and Majda [2]. Moreover, the sequence converges in $L^1_{\mathrm{loc}}(\mathbf{R}^2 \times [0,T])$ for any $T > 0$, and the limit $u(x,y,t)$ is a solution of (3). Using a similar argument as in Ref. [2], we can then dispense with the assumption of compact support on the initial data.

The entropy solution of (3) satisfies the following Kružkov entropy condition

$$\begin{aligned}\iint_{\mathbf{R}^2}\int_0^T \Big\{\phi_t|u-k| + F(u,k)\big(U\phi\big)_x + G(u,k)\big(V\phi\big)_y\Big\}\,dxdydt \\ - \iint_{\mathbf{R}^2} |u(T)-k|\phi(T)\,dxdy + \iint_{\mathbf{R}^2} |u(0)-k|\phi(0)\,dxdy \geq 0.\end{aligned} \tag{8}$$

where $F(u,k) = \operatorname{sgn}(u-k)(f(u)-f(k))$. We use $(U\phi)_x$ as a shorthand for the generalized derivative $\phi U_x + \phi_x U$.

We want to show that the limit solution $u(x,y,t)$ satisfies this entropy condition and that it hence is a unique entropy solution. The argument is a slight variation to that by Crandall and Majda [1]. For the approximate solutions we use the time interpolation

$$u_\Delta(x,y,t) = \begin{cases} \mathcal{S}_\delta^{f,U}\big(2(t-t_n)\big)u_{ij}^n(x,y), & \text{for } t\in[t_n, t_{n+1/2}), \\ \mathcal{S}_\delta^{g,V}\big(2(t-t_{n+1/2})\big)u_{ij}^{n+\frac12}(x,y), & \text{for } t\in[t_{n+1/2}, t_{n+1}). \end{cases}$$

The solution obtained after one sweep in either direction is the entropy solution of an equation similar to (2) and thus satisfies a corresponding one-dimensional entropy condition. Note that time now goes 'twice as fast'. We therefore introduce a modified test function $\tilde\phi(x,y,t) = \phi(x,y,2t)$. Then $u_j^n(x,t)$ satisfies

$$\begin{aligned}\int_{\mathbf{R}}\int_{t_n}^{t_{n+1/2}} \Big\{\tfrac12\phi_t|u_j^n(x,t)-k| + F_\delta(u_j^n(x,t),k)\big(U^\delta\phi\big)_x\Big\}\,dxdt \\ -\frac12\int_{\mathbf{R}}\big|u_j^n(x,t_{n+1/2}^-)-k\big|\phi(x,t_{n+1/2})\,dx + \frac12\int_{\mathbf{R}}\big|u_j^n(x,t_n^+)-k\big|\phi(x,t_n)\,dx \geq 0.\end{aligned}$$

A similar inequality is valid for the y-sweep

$$\begin{aligned}\int_{\mathbf{R}}\int_{t_{n+1/2}}^{t_{n+1}} \Big\{\tfrac12\phi_t|u_i^{n+\frac12}(y,t)-k| + G_\delta(u_i^{n+\frac12}(y,t),k)\big(V^\delta\phi\big)_y\Big\}\,dydt \\ -\frac12\int_{\mathbf{R}}\big|u_i^{n+\frac12}(y,t_{n+1}^-)-k\big|\phi(y,t_{n+1})\,dy + \frac12\int_{\mathbf{R}}\big|u_i^{n+\frac12}(y,t_{n+1/2}^+)-k\big|\phi(y,t_{n+1/2})\,dy \geq 0.\end{aligned}$$

We integrate the two inequalities over y and x, respectively, add them, and sum over n

$$\begin{aligned}\iint_{\mathbf{R}^2}\int_0^T \Big\{\tfrac12\phi_t|u_\Delta-k| + \chi_n F_\delta(u_\Delta,k)\big(U^\delta\phi\big)_x + (1-\chi_n)G_\delta(u_\Delta,k)\big(V^\delta\phi\big)_y\Big\}\,dxdydt \\ -\frac12\int_{\mathbf{R}}\big|u_\Delta(x,y,T)-k\big|\phi(x,y,T)\,dxdy + \frac12\int_{\mathbf{R}}\big|u_\Delta(x,y,0)-k\big|\phi(x,y,0)\,dxdy \\ \geq \frac12\sum_{n=1}^{2N}\int_{\mathbf{R}}\Big\{\big|u_\Delta(x,y,t_{n/2}^+)-k\big|\phi(x,y,t_{n/2}) - \big|u_\Delta(x,y,t_{n/2}^-)-k\big|\phi(x,y,t_{n/2})\Big\}\,dxdy.\end{aligned}$$

Here χ_n denotes the characteristic function of $\{(x,y,t)|t_n \leq t \leq t_{n+1/2}\}$ and $N\Delta t = T$. In the limit $n \to \infty$ we have that $\chi_n \to \frac{1}{2}$. The sum on the right-hand side reflects the projection operator used after each one-dimensional sweep. As the spatial discretization tends to zero, the projection operator tends to the identity operator and the right-hand side disappears. We then let the parameters δ in the approximation of flux and velocity tend to zero. By using the bounded convergence theorem for Lebesgue integrals we obtain the entropy condition (8). Thus we have proved the following lemma:

Lemma 3.4. *The limit solution $u(x,y,t)$ is a weak entropy solution of* (3)*; that is, it fulfills the entropy condition* (8)*.*

In the case of time dependent velocities, the above analysis goes through with the obvious modifications. Similarly, extending these results to arbitrary space dimension is also straightforward. The results can be summarized in a theorem:

Theorem 3.5. *Let u_0 be a bounded function with bounded total variation. Let f_i be Lipschitz continuous functions and $V_i(x,t)$ be bounded functions that are Lipschitz continuous in x. Moreover, assume that for each finite $T > 0$ there are a finite number of points $\tau < T$ such that* $\operatorname{sgn} V_i(x,\tau^-) \neq \operatorname{sgn} V_i(x,\tau^+)$*. Then the sequence of approximate solutions defined by*

$$u^n(x,t) = \left[\pi S_\delta^{f_d,V_d}(\Delta t) \cdots \pi S_\delta^{f_1,V_1}(\Delta t)\right]^n \pi u_0(x)$$

converges to the unique entropy solution of (1)*.*

4. Numerical Examples

The front tracking method has been tested on various examples. Here we present three problems. The first is a simple counterclockwise rotation of a cylinder. Its purpose is to illustrate the two error mechanisms in the dimensional splitting; the splitting and the projection. The second example introduces an important application of the method; solution of equations on curvilinear grids. Although both examples are simple advection problems, this is by no means a prerequisite for the method. The two examples were chosen merely for their simplicity. The front tracking method was developed for, and is most successfully applied to *nonlinar* problems. Linear advection problems are in many aspects a worst case for the method, since they contain no self-sharpening that counteracts the smearing introduced by the projection operator.

The third example is nonlinear and has a stronger flavour of real-life. It models water injection in a homogeneous petroleum; a two-phase flow process. Neglecting capillary forces, the process is described by a hyperbolic–elliptic system. Similar examples with capillary forces included (and with a real pressure solver) can be found in Karlsen *et al.* [6]. There the front tracking method constitutes an important part of a novel methodology for obtaining the correct balance of advection and diffusion in petroleum reservoirs. See also Evje *et al.* [3] for applications of the method to degenerate hyperbolic–parabolic problems.

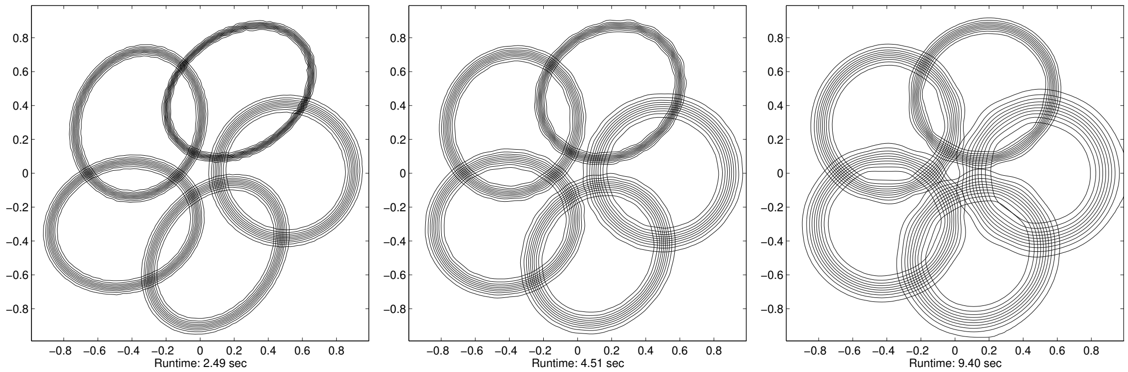

FIGURE 1. Example 1. Contour plots of the cylinder at five equally spaced points in time during the first rotation. The number of time steps is 20, 40, and 80 from left to right corresponding to CFL numbers 15.7, 7.9, and 3.9, respectively.

Example 1: A Rotating Cylinder. Consider a cylinder that rotates counterclockwise around the origin in a rectangular domain $[-1,1] \times [-1,1]$,

$$u_t - yu_x + xu_y = 0, \qquad u(x,y,0) = u_0(x,y),$$

where

$$u_0(x,y) = \begin{cases} 1, & \text{if } (x-0.5)^2 + y^2 \leq 0.16 \\ 0, & \text{otherwise.} \end{cases}$$

By introducing cylindrical coordinates (see Example 2 below), this problem can be transformed to a family of one-dimensional problems and solved exactly. However, since the problem is a pure linear advection problem, it allows us to study the two factors contributing to the total error; the errors introduced by the splitting and by the projection. We have earlier pointed out that the front tracking method is unconditionally stable. Hence very large time steps can be used to reduce the number of splitting steps. Although this is favourable in terms of computer efficiency, it obviously leads to large splitting errors. On the other hand, the number of projections is reduced and hence the corresponding smearing.

In Figure 1 we have plotted the contours of the cylinder at five equally spaced points in time during one revolution using 20, 40, and 80 time steps. The number of unknowns in each direction is 100. The effect described above is clearly evident. With 20 time steps there is little smearing after one rotation. However, the cylinder appears rather deformed during the revolution. On the other hand, using 80 time steps gives an adequate representation of the shape throughout the rotation, but also introduces considerable smearing due to the large number of projections.

Figure 2 shows the error in L^1 and L^2-norm after one revolution versus runtime for CFL numbers 2, 4, 8, and 16. The norms were computed using a fourth order numerical quadrature on each rectangle in the grid. The number of unknowns in each direction was $25 \cdot 2^n$, for $n = 0, \ldots, 4$. Based on the measurements of the error, we can determine

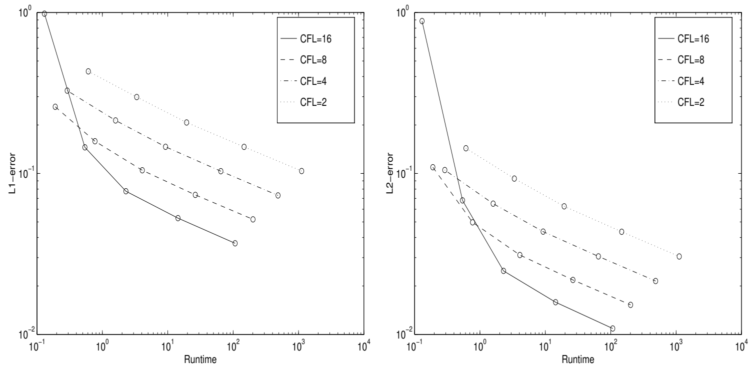

FIGURE 2. Example 1. Errors in L^1-norm (left) and L^2-norm (right) after one rotation versus runtime for CFL numbers 2, 4, 8, and 16.

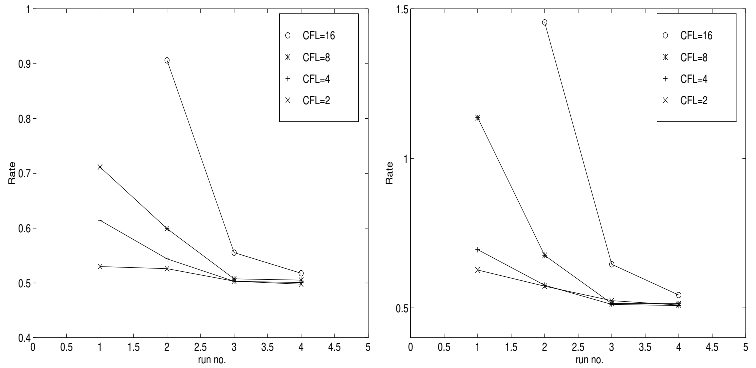

FIGURE 3. Example 1. Instantaneous convergence rates for error in L^1-norm (left) and L^2-norm (right) after one rotation versus runtime for CFL numbers 2, 4, 8, and 16.

instantaneous convergence rates. If e_n denotes the error for run n, then the instantaneous convergence rate is defined as $r_n = \log_2(e_n/e_{n+1})$. Plots of observed rates are given in Figure 3. Notice that the highest efficiency is observed for CFL number 16 (except on the coarsest grid). Furthermore, the rates are well above $\frac{1}{2}$ for the coarser grids, but seem to go asymptotically to $\frac{1}{2}$ as the grid is refined. The rates are not surprisingly low, as there is no self-sharpening effect in the equation to counteract the $\mathcal{O}(\Delta x^{1/2})$ smearing introduced by the projection operator. For nonlinear equations a higher rate can be observed, see Ref. [10].

Example 2: Curvilinear Grids. The second example introduces an important application of the method—computations on curvilinear grids. For simplicity consider the linear advection equation

$$u_t + U(x,y)u_x + V(x,y)u_y = 0, \qquad u(x,y,0) = u_0(x,y),$$

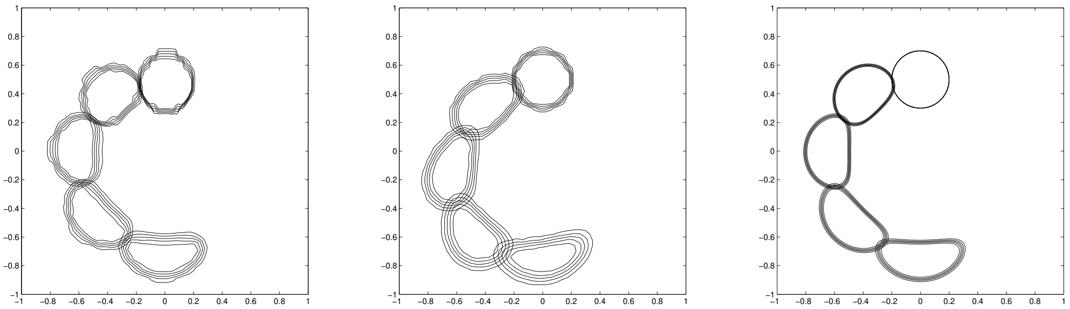

FIGURE 4. Example 2. Snapshots of solution during time interval $t \in [0, \pi]$. (Left) Cylindrical 15*150 grid with 4 time steps. (Middle) Cartesian 50*50 grid with 8 time steps. (Right) A fine grid solution on a 800*800 Cartesian grid.

where the velocities are superpositions of the rotation from Example 1 and a radial movement ($a = 0.05$)

$$U(x, y) = -y + \frac{ax}{x^2 + y^2}, \qquad V(x, y) = x + \frac{ay}{x^2 + y^2}.$$

The initial function is equal one inside a circle with radius 0.2 centred at $(0, 0.5)$ and zero elsewhere. The cylinder will rotate around the origin and at the same time be deformed due to the decreasing radial velocity component. Now, introduce cylindrical coordinates (r, θ) by the coordinate transform

$$x = r\cos\theta, \qquad y = r\sin\theta.$$

In the new coordinates the equation becomes

$$u_t + R(r, \theta)u_r + \Theta(r, \theta)u_\theta = 0,$$

where

$$\begin{aligned} R(r, \theta) &= \cos\theta\, U(r\cos\theta, r\sin\theta) + \sin\theta\, V(r\cos\theta, r\sin\theta) \\ \Theta(r, \theta) &= r^{-1}\sin\theta\, U(r\cos\theta, r\sin\theta) + r^{-1}\cos\theta\, V(r\cos\theta, r\sin\theta). \end{aligned}$$

We thus get the simple advection equation $u_t + u_r + (a/r)u_\theta = 0$. To avoid the singularity at the origin, the computational domain is chosen equal $[0.2, 1.0] \times [0, 2\pi]$, and we impose periodic boundary conditions at $\theta = 0$ and $\theta = 2\pi$. Figure 4 shows five snapshots of the solution in the time interval $t \in [0, \pi]$ computed on a 15*150 grid with 4 time steps and on a 50*50 Cartesian grid with 8 time steps. For reference, a solution computed on a fine Cartesian grid has been included. Not surprisingly, we observe that the curvilinear grid gives a superior resolution of the movement of the cylinder. On the other hand, the grid cells have approximately equal area and give almost the same amount of smearing of the discontinuities.

Example 3: Water Injection in An Oil Reservoir. The final example describes water injection into a homogeneous and horizontal oil field. The flow of oil and water is assumed to be immiscible and incompressible. If we choose total Darcy velocity V, total fluid pressure p, and water saturation s as primary variables, the displacement of oil by water is governed by a coupled system of nonlinear partial differential equations. We have the elliptic pressure equation

$$\nabla\big((\lambda_w + \lambda_o)\nabla p\big) = 0,$$

where λ_w and λ_o are the mobilities (relative permeability k_{ri} divided by viscosity μ_i) of water and oil and are assumed to be known functions of the saturation. As a simple model we use $\lambda_w(s) = s^2$ and $\lambda_o(s) = (1-s)^2$.

The pressure equation is coupled via the total Darcy velocity $V = -(\lambda_w + \lambda_o)\nabla p$ to the hyperbolic saturation equation

$$s_t + V \cdot \nabla f(s) = 0,$$

where the fractional flow function $f = f(s)$ is given by the expression

$$f = \frac{\lambda_w}{\lambda_w + \lambda_o}.$$

In the saturation equation we have neglected diffusion due to capillary forces. The system is constrained by appropriate initial and boundary conditions; here we will use $s = 0$ initially and 'no flow' boundary conditions, that is, $V \cdot n = 0$ on the boundary. In the saturation equation, the production wells are modelled as outflow boundaries and the injection wells as inflow boundaries with a saturation kept fixed at 1.

A sequential time stepping procedure is used to decouple the equations. First the pressure equation is solved with the initial saturation as input to generate a total velocity field. Subsequently, the velocity field is held constant when solving the saturation equation. Then the pressure is recomputed, and so on. This strategy is common and reflects the different nature of the two equations; see Refs. [11] for an analysis of this procedure.

Instead of solving the pressure equation by a numerical method, we use a simple analytic approximation to the pressure: Assume that each well is a point source. From well number i located at (x_i, y_i) we add the contribution $\frac{1}{2}q_i \ln((x-x_i)^2 + (y-y_i)^2)$ to the total pressure, where q_i is a constant (positive for injection and negative for production). The Darcy velocity becomes $V = \nabla \sum_i \frac{1}{2}q_i \ln((x-x_i)^2 + (y-y_i)^2)$. Although crude, this approximation is reasonable away from each well.

The computational domain is $[0,1] \times [0,1]$. We have used one injection well and four production wells; the strength ratio is 4:1. In Figure 5 . To reduce the error contribution from the velocity approximation, we start with an initial saturation surrounding the injection well, see Figure 5. We show the water saturation as contour plots (with ten contours) at times $t = 0.0$ and 0.3. To reach final computing time 0.3 we have used 3 time steps on a 100*100 grid, corresponding to CFL numbers in the range 10–20 away from the wells. The reference solution is generated on a 500*500 grid using 60 time steps.

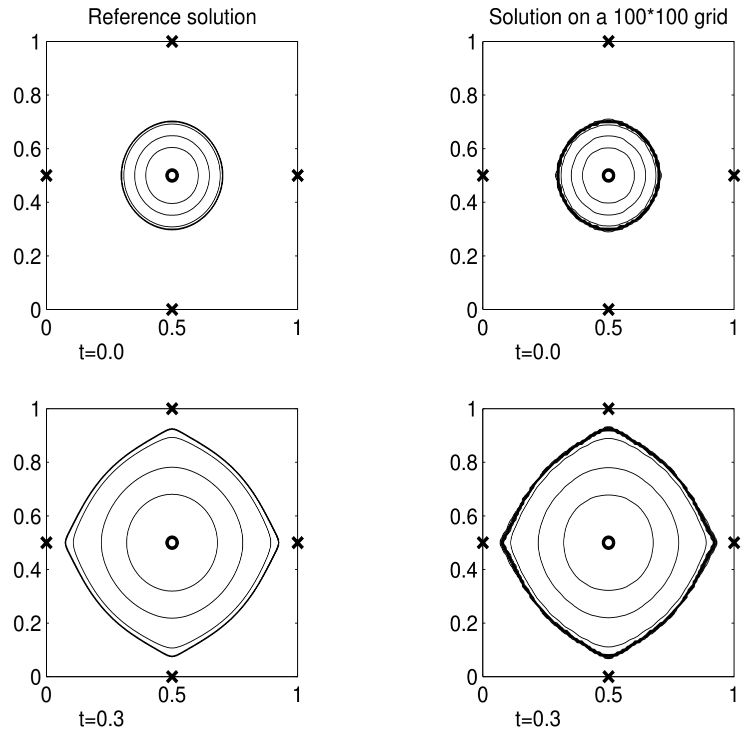

FIGURE 5. Example 3. Saturation profiles initially (top) and at time $t = 0.3$ (bottom). The injection well in the centre is marked by an 'o' and production wells by an 'x'.

Acknowledgement. I thank Vidar Haugse, Helge Holden, Kenneth Hvistendahl Karlsen, and Nils Henrik Risebro for many fruitful discussions.

REFERENCES

[1] M. G. Crandall and A. Majda. The method of fractional steps for conservation laws. *Numer. Math.*, 34:285–314, 1980.

[2] M. G. Crandall and A. Majda. Monotone difference approximations for scalar conservation laws. *Math. Comput.*, 34(149):1–21, Jan. 1980.

[3] S. Evje, K. H. Karlsen, K.-A. Lie, and N. H. Risebro. Front tracking and operator splitting for nonlinear degenerate convection–diffusion equations. Preprint series, The Mittag–Leffler Institute, Oct. 1997.

[4] H. Holden, L. Holden, and R. Høegh-Krohn. A numerical method for first order nonlinear scalar conservation laws in one-dimension. *Comput. Math. Applic.*, 15(6–8):595–602, 1988.

[5] H. Holden and N. H. Risebro. A method of fractional steps for scalar conservation laws without the CFL condition. *Math. Comput.*, 60(201):221–232, Jan. 1993.

[6] K. H. Karlsen, K.-A. Lie, N. H. Risebro, and J. Frøyen. A front tracking approach to a two-phase fluid flow model with capillary forces. To appear in a special issue of *In Situ*.

[7] S. N. Kružkov. First order quasi-linear equations in several independent variables. *Math. USSR Sbornik*, 10(2):217–243, 1970.

[8] R. J. LeVeque. High-resolution conservative algorithms for advection in incompressible flow. *SIAM J. Numer. Anal.*, 33:627–665, 1996.

[9] K.-A. Lie. A front tracking method for one-dimensional nonlinear advection equations with variable coefficients. Preprint. mathematics, Norwegian University of Science and Technology, Trondheim, Norway, 1997.

[10] K.-A. Lie, V. Haugse, and K. H. Karlsen. Dimensional splitting with front tracking and adaptive grid refinement. Preprint. Mathematics 2, Norwegian University of Science and Technology, Trondheim, Norway, 1996. Available at the URL `http://www.math.ntnu.no/conservation/`.

[11] H. J. Schroll and A. Tveito. Local existence and stability for a hyperbolic–elliptic system modeling two–phase reservoir flow. Preprint 136, RWTH Aachen, 1997.

(Knut–Andreas Lie)
Department of Mathematical Sciences
Norwegian University of Science and Technology
N-7034 Trondheim, Norway
E-mail address: `andreas@math.ntnu.no`